physica status solidi

pss

www.pss-journals.com

reprint

WILEY-VCH

EarlyView publication on wileyonlinelibrary.com
(issue and page numbers not yet assigned;
citable using Digital Object Identifier – **DOI**)

Phys. Status Solidi B, 1–7 (2011) / **DOI** 10.1002/pssb.201046402

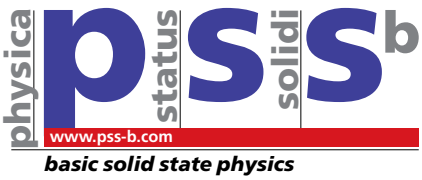

Weak ferromagnetism in cobalt oxalate crystals

E. Romero*[,1], M. E. Mendoza[1], and R. Escudero[2]

[1] Instituto de Física, Benemérita Universidad Autónoma de Puebla, Apartado Postal J-48, 72570 Puebla, México
[2] Instituto de Investigaciones en Materiales, Universidad Nacional Autónoma de México, Apartado Postal 70-360, 04510 México DF, México

Received 22 July 2010, revised 17 November 2010, accepted 17 November 2010
Published online 18 January 2011

Keywords Antiferromagnetic materials, Cobalt oxalate, Coprecipitation reactions, Molecular magnets

* Corresponding author: e-mail eromero@sirio.ifuap.buap.mx, Phone: +52-222-2295610, Fax: +52-222-2295611

Microcrystals of diaquocobalt(II) oxalate have been synthesized by the coprecipitation reaction of aqueous solutions of cobalt(II) bromide and oxalic acid. Chemical analysis and thermal experiments revealed that there is only one phase present. X-ray powder diffraction studies show that this compound is orthorhombic with space group *Cccm*. Molar susceptibility versus temperature measurements show the existence of an antiferromagnetic ordering; however, the hysteresis measured in magnetization measurements as a function of magnetic field reveals a weak ferromagnetic behavior.

1 Introduction Oxalate dihydrates containing divalent $3d$ transition elements, with general formula $MC_2O_4 \cdot nH_2O$, where M is a metallic 2+ ion [1–11], exhibit quasi-one-dimensional magnetic behavior characterized by a dominant magnetic correlation along oxalate–metal-ion chains. Kurmoo [12] has reported a weak antiferromagnetic (AF) interaction in these compounds. However, it is expected that in systems like the aforementioned oxalates, with many close chains [13], the intra- and interchain magnetic interactions cant the spins, distorting the antiferromagnetic order and producing also a weak ferromagnetism (WF). At low temperatures, the WF behavior will be presumably more pronounced.

Cobalt oxalate dihydrate is a quasi-one-dimensional magnetic compound useful for searching for the existence of WF at low temperature because it crystallizes in two allotropic forms [14]: α-monoclinic, space group $C2/c$, $a = 11.775$ Å, $b = 5.416$ Å, $c = 9.859$ Å, and $\beta = 127.9°$, and β-orthorhombic, $Cccm$, $a = 11.877$ Å, $b = 5.419$ Å, and $c = 15.624$ Å. Both structures are formed by identical infinite chains of $[CoC_2O_4 \cdot 2H_2O]$ units; the difference between them lies in the relative displacement of adjacent chains along the b-axis [15–18]. Each Co^{2+} ion is surrounded by a distorted oxygen octahedron, where four oxygens belong to the oxalate anions and the other two to the water molecules. The more stable α structure is the most studied. Its magnetic structure [19] has been described as two interpenetrating AF sublattices belonging to the Shubnikov group P_bC, with parameters a, $2b$, and c. It was found that below the Néel temperature $T_N = 6.1$ K, three-dimensional AF long-range order exists, corresponding to a collinear magnetic structure with $k = [0, 1/2, 0]$ and magnetic moments aligned parallel to the a-axis.

In this paper, we will report results on the synthesis, crystal structure, and magnetic measurement of the orthorhombic β-$CoC_2O_4 \cdot 2H_2O$ microcrystals. It was determined by M–H measurements from 2 to 200 K that this phase exhibits WF ordering at $T < 7.5$ K.

2 Experimental methods The synthesis of orthorhombic β cobalt oxalate dihydrate was carried out by coprecipitation reaction of aqueous solutions of cobalt(II) bromide 0.1 M (Aldrich, 99%) and oxalic acid 0.00625 M (Aldrich, $\geq$ 99%), according to the chemical equation

$$H_2C_2O_{4(aq)} + CoBr_{2(aq)} \rightarrow CoC_2O_4 \cdot 2H_2O_{(s)} + 2HBr_{(aq)}.$$

The precipitates were filtered and dried at room temperature.

Morphological analyses were performed with a scanning electron microscope (SEM, Cambridge Leica Stereoscan 440). Powder X-ray diffraction (XRD) patterns were

acquired using a Siemens D5000 diffractometer, operating in the Bragg–Brentano geometry with λ(Cu–Kα) = 1.541 Å and 2θ scan = 10–70°, with a step size of 0.02°. Thermogravimetric (TG) and differential thermal analysis (DTA) curves were obtained in a SDT-TA Instruments model 2960, in air atmosphere with heating rate of 5 °C/min from room temperature up to 600 °C. Heat capacity was measured between 2 and 300 K in a Quantum Design "Physical Property Measurement System" (PPMS). Magnetization measurements were performed in a Quantum Design "Magnetic Property Measurement System" (MPMS) SQUID magnetometer (MPMS-5). Zero field cooling (ZFC) and field cooling (FC) cycles were performed at a magnetic intensity of 1 T, in the range from 2 to 300 K. Isothermal magnetization measurements $M(H)$ were obtained at 2, 50, 100, 160, and 200 K. The diamagnetic contribution calculated from Pascal's constants [20] was $\chi_{Di} = -72 \times 10^{-6}\,cm^3/mol$.

3 Results and discussion

3.1 Synthesis and morphology Five polycrystalline samples were obtained using different reaction times (see Table 1). Pink cobalt oxalate dihydrate microcrystals were obtained after dry precipitation at room temperature. Chemical analyses by digestion using inductively coupled plasma–optical emission spectrometry (ICP-OES) and by combustion using thermal conductivity–infrared (TCD/IR) measurements and pyrolysis–IR measurements, give the composition in weight of 35% of cobalt, 13.21% of carbon, 2.45% of hydrogen, and 54.92% of oxygen. The morphology shown by all the precipitates is tubular like (inset in Fig. 1), generated by self assembly of needle-like microcrystals as shown in Fig. 1. The observed microtubes have an average length (L) and a diameter (D) in the ranges from 16 to 146.2 and 0.6 to 3.8 μm, respectively. This morphology is not the usual one for the cobalt oxalates prepared by precipitation methods from homogeneous solutions without additives.

Some reports concerning the morphology of 3d-ion oxalates prepared by precipitation reactions have been published; Pujol et al. [21] have found that cobalt oxalate dihydrate crystals present a rod-like morphology. They used as reactant solutions cobalt nitrate and sodium oxalate. Jongen et al. [22] have also obtained copper oxalate with controlled morphology from cushion- to rod-like crystals, using solutions of copper nitrate and sodium oxalate, adding a polymer at different concentrations. These authors show that the mechanism of growth is by self assembly, guided by the copper oxalate crystal structure. Additionally, nanorods of nickel oxalate were synthesized using solutions of nickel nitrate and ammonium oxalate adding a cationic surfactant (cetyltrimethylammonium bromide, CTAB) [23]. Negative surface charge on the nanorods was observed; it has a bearing on the growth of the rods along the cross section, especially with surfactant molecules having positively charged head groups (CTAB).

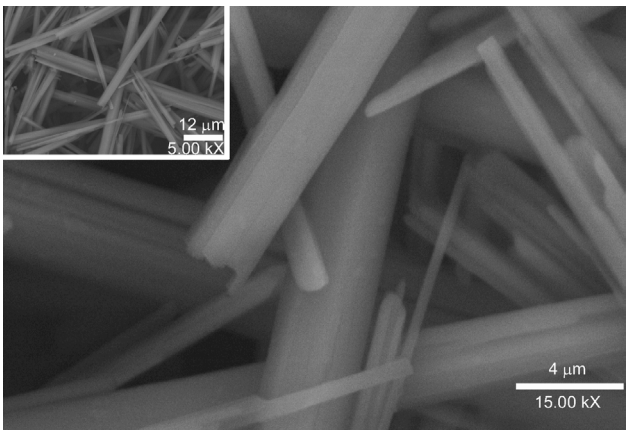

Figure 1 SEM micrograph of cobalt oxalate needle-like crystallites forming tubular microcrystals, for sample S4.

It is known that in crystal growth in aqueous solutions, there is a correlation between the ionic strength of the solution and the kinetics of crystal faces [24]. In order to explain the morphology of our orthorhombic β-$CoC_2O_4 \cdot 2H_2O$ crystals obtained in this work, and compare with that reported by Pujol, we calculated the ionic strength of the solutions in both cases using the Debye equation $I = 1/2 \sum C_i Z_i^2$, where I is the ionic strength and C_i and Z_i are the concentration and charge of ion i, respectively [25]. Whereas Pujol et al. [21] used cobalt nitrate 0.0052 M and sodium oxalate 0.005 M, in our work we used cobalt bromide 0.00625 M and oxalic acid 0.1 M. The calculated ionic strengths were 0.0306 M [21] and 0.3187 M, (this work) with a difference between them of about one order of magnitude.

Additionally, in our work the pH at the end of the reaction was 1.5; this high concentration of H^{+1} ions would then assemble on the negative surface of the growing cobalt oxalate crystals, and the high ionic strength of the solutions would screen the self assembly of crystallites, giving as a final result the tubular-like morphologies.

Table 1 Polycrystalline samples obtained using different reaction times. TG denotes growth time, D and L are average diameter and length of the particles, respectively.

Sample	TG	D (μm)	L (μm)
S1	12 min	0.6	16.0
S2	12 h	1.4	53.3
S3	24 h	1.5	55.4
S4	40 h	2.1	79.9
S5	7 days	3.8	146.2

3.2 Diffraction pattern The monoclinic α-phase of $CoC_2O_4 \cdot 2H_2O$ is characterized by the presence of a doublet peak in the XRD powder diagram; the peaks are at $2\theta = 18.695°$ and 19.076°, respectively [18].

Figure 2a displays the XRD powder diffraction pattern of the sample S4 (blue pattern), in good agreement with the reported pattern (red lines in Fig. 2b) for the orthorhombic

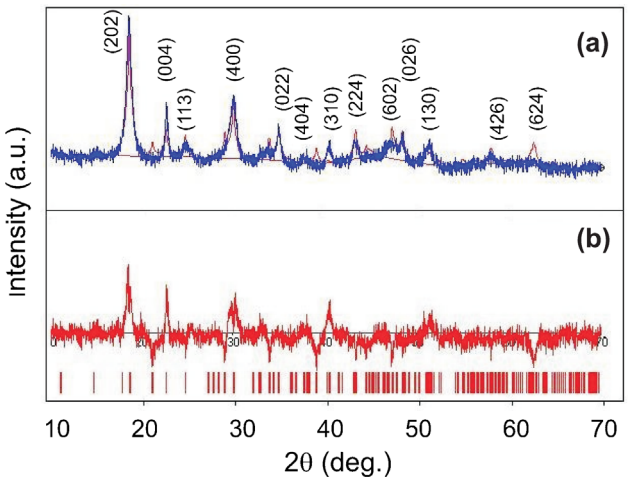

Figure 2 (online color at: www.pss-b.com) (a) X-ray powder diffraction data of sample S4 (blue pattern) and Miller indices for orthorhombic space group *Cccm* (JCPDS file: 25-0250). The theoretical structural refinement (red pattern) was performed using the Win-Rietveld software. (b) The refinement difference.

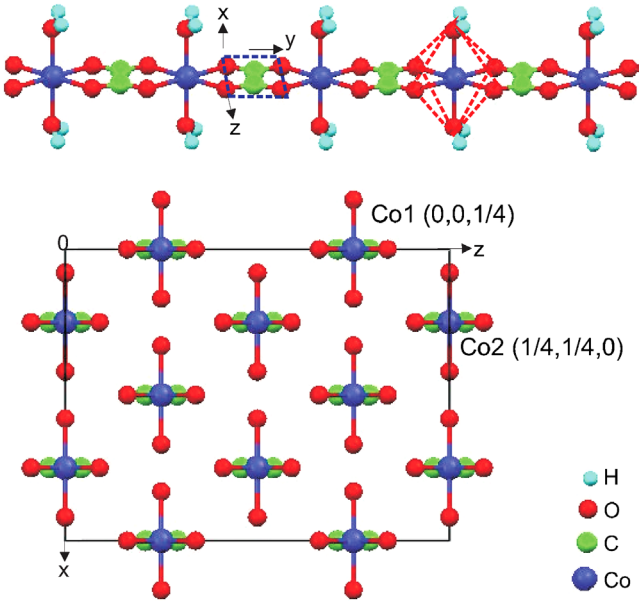

Figure 3 (online color at: www.pss-b.com) Cobalt oxalate unit cell of the orthorhombic β-phase (JCPDS file 25-0250, space group *Cccm*). There are eight cobalt atoms located in two non-equivalent positions designated as Co1 and Co2.

β-phase of cobalt oxalate dihydrate (JCPDS file: 25-0250). In all other samples (S1, S2, S3, and S5) the same phase was identified.

Rietveld refinement [26] of the pattern was performed using the Win-Rietveld software, the background was estimated by linear interpolation, and the peak shape was modeled by a pseudo-Voigt function. Unit-cell parameters used were $a = 11.877$ Å, $b = 5.419$ Å, and $c = 15.624$ Å [14]. The atomic positions were those reported by Deyrieux and Péneloux for iron oxalate [17]: 4Co $\left(\frac{1}{4},\frac{1}{4},0\right)$, 4Co $\left(0,0,\frac{1}{4}\right)$, $8C_{oxalate}$ $\left(\frac{1}{4},\frac{3}{4},0.041\right)$, $8C_{oxalate}$ $\left(0,\frac{1}{2},0.291\right)$, $16O_{oxalate}$ $\left(\frac{1}{4},0.941,0.089\right)$, $16O_{oxalate}$ (0,0.691, 0.339), $8O_{water}$ $\left(0.419,\frac{1}{4},0\right)$, and $8O_{water}$ $\left(0.169\ ,0,\frac{1}{4}\right)$. The weighted profile and expected residual factors obtained by the Rietveld refinement were $R_{wp} = 20.04$ and $R_{exp} = 9.95$. The refined cell parameters determined for the cobalt oxalate orthorhombic phase in all samples were $a = 11.879(4)$ Å, $b = 5.421(2)$ Å, and $c = 15.615(6)$ Å. A schematic representation of the unit cell is shown in Fig. 3. In this figure there are two non-equivalent positions for the cobalt ions, designated as Co1 and Co2; each cobalt ion is shifted with respect to the other by a translation vector $\left(\frac{1}{2},\frac{1}{2},0\right)$.

Finally, the mean crystallite dimension (D) for the sample was calculated with the Scherrer Eq. (1) using the (202) peak:

$$D = \frac{0.9\lambda}{(B-b)\cos\theta}, \tag{1}$$

where λ is the wavelength of the radiation, B is the width of the diffraction line at half-intensity maximum, b is the instrumental broadening (0.05), and θ is the diffraction angle. The calculated values were 21.4 nm for the S1, S2, and S3 samples, 22.7 nm for the S4 sample, and 26.4 nm for the S5 sample.

3.3 Thermal analysis TG studies of all samples of $CoC_2O_4 \cdot 2H_2O$ have shown two steps of weight loss, the first one occurring at about 150 °C and the second one at about 270 °C. Figure 4 presents the TG curve for sample S4. In the first step the weight loss of 18.5% corresponds to two water molecules; this is according to the theoretical value of 19.7%. The DTA curve associated with this process shows an endothermic peak at about 145 °C. The dehydration

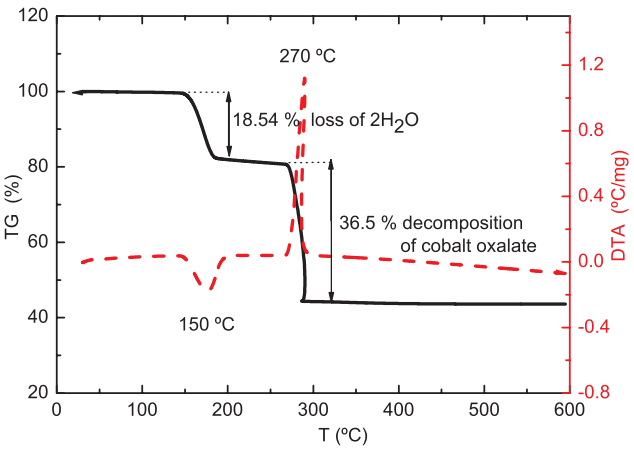

Figure 4 (online color at: www.pss-b.com) TG (solid line)/DTA (dashed line) curves for $CoC_2O_4 \cdot 2H_2O$ (sample S4) at 5°C/min heating rate.

reaction is

$$CoC_2O_4 \cdot 2H_2O_{(s)} \rightarrow CoC_2O_{4(s)} + 2H_2O. \quad (2)$$

The weight loss of 36.4% in the second step may be attributed to the decomposition of the anhydrous cobalt oxalate to obtain cobalt oxide. This agrees with the theoretical value [27]. The corresponding DTA curve shows an exothermic peak at about $T = 267^{\circ}C$. The decomposition reaction in this step can be written as

$$3CoC_2O_{4(s)} + 2O_2 \rightarrow Co_3O_{4(s)} + 6CO_2. \quad (3)$$

It is important to observe that the absence of any additional peak in the TG and DTA curves indicates the high purity of the cobalt oxalate samples.

3.4 Heat capacity The heat capacity of β-$CoC_2O_4 \cdot 2H_2O$ (sample S4) is plotted as a function of temperature in Fig. 5. The most important feature is the sharp λ-peak occurring at about 7.5 K. It is important to mention that for α-$CoC_2O_4 \cdot 2H_2O$ the λ-peak was reported at about $T = 6.23$ K, indicating the onset of long-range magnetic order [28] and consistent with the Néel temperature $T_N = 6.1 \pm 0.1$ K found in deuterated cobalt oxalate [19]. So, for β-$CoC_2O_4 \cdot 2H_2O$, we report a Néel temperature of about 7.5 K.

3.5 Magnetic measurements The molar susceptibility as a function of temperature, $\chi(T)$, for the five samples S1–S5 is shown in Fig. 6. It was measured at a magnetic field of 1 T in both ZFC and FC modes. All samples have almost the same behavior; at low temperature the magnetic susceptibility values are small; they increase rapidly as the temperature increases up to a maximum close to 24 K, see inset of Fig. 6. As the temperature is raised, $\chi(T)$ smoothly decreases up to a minimum at room temperature. Although the χ_{max} values are different in all samples (varying in the range of 3.3×10^{-2}–4.08×10^{-2} cm^3/mol), they are similar to those reported for α-$CoC_2O_4 \cdot 2H_2O$, where $\chi_{max} = 3.6 \times 10^{-2}$ cm^3/mol [28]. From room temperature to 100 K a Curie–Weiss behavior clearly can be fitted.

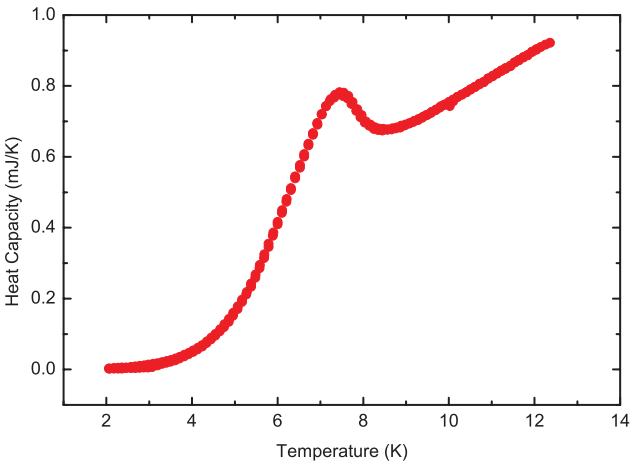

Figure 5 (online color at: www.pss-b.com) Heat capacity of β-$CoC_2O_4 \cdot 2H_2O$, sample S4. Peak at $T = 7.5$ K. This λ-peak represents the AF transition with onset at about 8.2 K, maximum at 7.5 K.

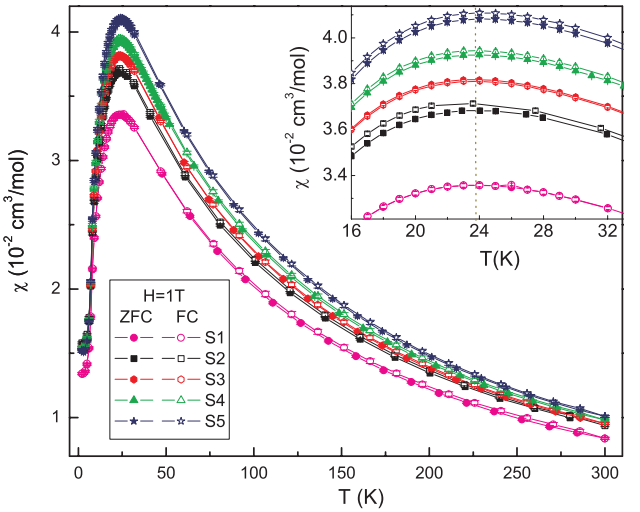

Figure 6 (online color at: www.pss-b.com) Molar susceptibility $\chi(T)$ of five samples of β-$CoC_2O_4 \cdot 2H_2O$, with maximum at 24 K, measured for ZFC and FC modes, with $H = 1$ T. Full colors (solid symbols) represent ZFC measurements, whereas open symbols represent the FC mode.

The maximum of the susceptibility at $T_{max} = 24$ K is a typical behavior of the susceptibility occurring in low-dimensional antiferromagnets [12, 29]; this curve is correctly predicted by

$$\frac{\chi_{max}|J|}{g^2\mu_B^2} = 0.07346, \quad (4)$$

at

$$\frac{k_B T_{max}}{|J|} = 1.282; \quad (5)$$

with $g = 2$ (for $3d$ ions), $\mu_B = 9.27 \times 10^{-24}$, and $k_B = 1.38 \times 10^{-23}$, we obtained a value $|J|/k_B = 18.72$ K, i.e. $|J| = 1.6$ meV.

In the case of nickel oxalate chains, Keene et al. [10] have modeled the behavior of an antiferromagnetically coupled chain of quantum spins by a polynomial approximation (6).

$$\chi_{cal} = \frac{N\mu_B^2 g^2}{k_B T}\left[\frac{A + Bx^2}{C + Dx + Ex^3}\right], \quad (6)$$

where $x = |J|/k_B T$. Using this model for the molar susceptibility of β cobalt oxalate, χ_{exp} (solid line) in Fig. 7, a good fit (dashed line) is obtained with $|J|/k_B = 18.72$ K, T (2–300 K), $g = 2.51$, $A = 1.3667$, $B = 1.36558$, $C = 1$, $D = 2.3018$, and $E = 5.7448$.

The maximum shown in the susceptibility in Figs. 6 and 7 is a characteristic feature of the effect of spin

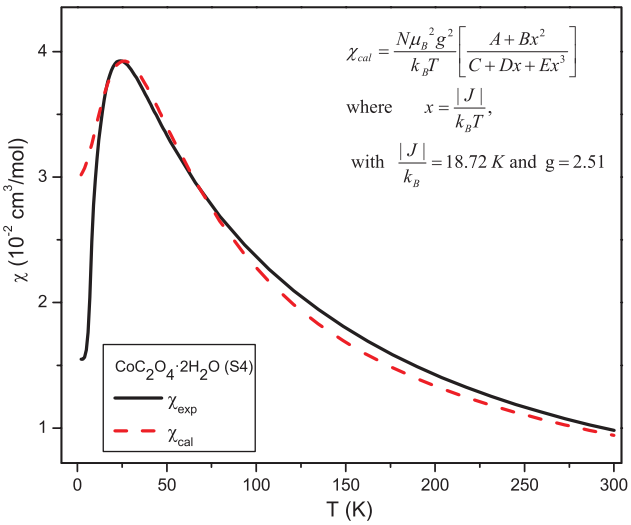

Figure 7 (online color at: www.pss-b.com) Molar susceptibility ($\chi_{exp}(T)$, solid line) of β-$CoC_2O_4 \cdot 2H_2O$ (sample S4) and the fit ($\chi_{cal}(T)$, dashed line) for antiferromagnetically coupled chain of quantum spins.

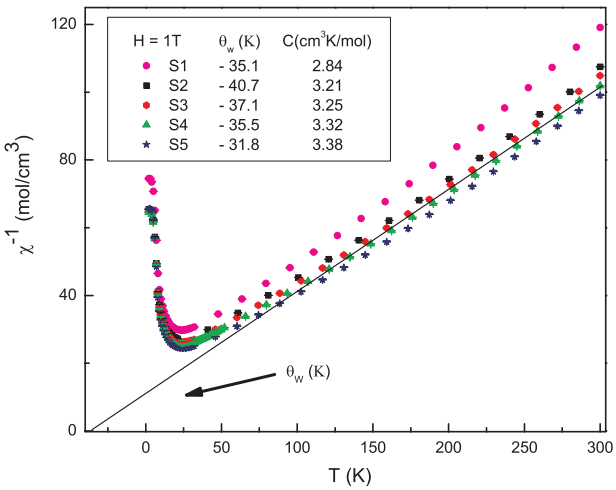

Figure 8 (online color at: www.pss-b.com) Inverse susceptibility $\chi^{-1}(T)$ corresponding to five samples. The Weiss temperature θ_ω changes from −35.8 to −40.7 K. The Curie constant also changes from 2.84 to 3.38 cm^3 mol^{-1} K.

fluctuations as described by the Heisenberg model [5]. The inset of Fig. 6 shows the molar susceptibility versus temperature from 16 to 32 K. Here, FC and ZFC modes present a small irreversibility that gives a hysteretic behavior at about 30 K with the maximum at about 24 K. This irreversibility corroborates the spin fluctuation characteristics at this temperature. At high temperatures the system tends clearly to be in a paramagnetic state. When the temperature decreases, thermal energy will be small and spin fluctuations tend to be canceled and aligned in a minimum-energy configuration.

Our results are similar to those reported for oxalate–cobalt(II) complexes [7, 30, 31]. However, our experimental observations show that this broad maximum may be due to the competition of two different magnetic orderings, an uncompensated antiferromagnetism and consequently a weak ferromagnetism.

In Fig. 8, there is shown a plot of the inverse of susceptibility, χ^{-1}, as a function of temperature at $H = 1$ T, for all samples. The analysis of these measurements was performed by fitting a Curie–Weiss behavior above 100 K, where the fit parameters: Weiss temperature θ_ω and Curie constant C, vary from −31.8 to −40.7 K and from 2.84 to 3.38 cm^3 mol^{-1}, respectively.

These data permit us to calculate the effective magnetic moment μ_{eff} per mole, according to the equation $\mu_{eff} = 2.84C^{1/2} = 2.84[\chi(T-\theta_\omega)]^{1/2}$. In Fig. 9, the effective number of Bohr magnetons at room temperature for each sample (S1–S5) is different (4.76, 5.07, 5.09, 5.15, and 5.19 μ_B). However, it is in agreement with reported values in studies of layered transition metal oxalates [32], where for octahedrally coordinated cobalt(II) with a $^4T_{1g}$ ground term the observed moment is typically 4.7–5.2μ_B.

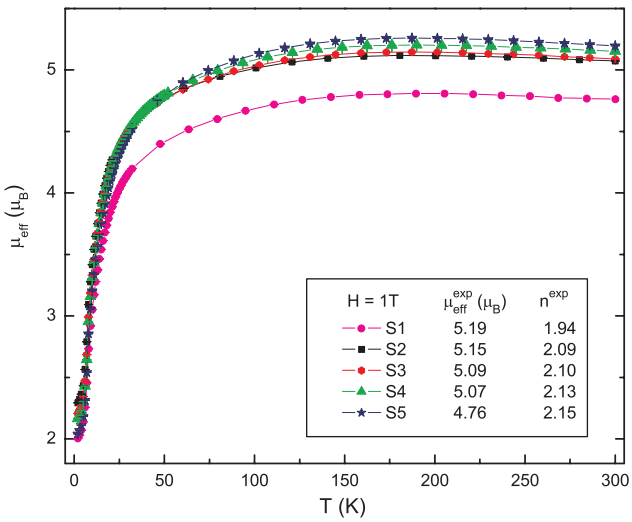

Figure 9 (online color at: www.pss-b.com) Effective Bohr magnetons, μ_{eff} per mole, as a function of temperature. At room temperature the values are between 4.76μ_B and 5.15μ_B. n is the number of unpaired electrons.

After calculation of μ_{eff}, the number of unpaired electrons n in β-$CoC_2O_4 \cdot 2H_2O$, using $\mu_{eff} = g[n(n+1)]^{1/2}$, can be calculated. Those values for each sample are in the range of 1.94–2.15.

The decrease in $\mu_{eff}(T)$ on cooling and the large negative Weiss temperature indicate an AF coupling between neighboring ions, for all samples S1–S5.

It is important to mention that short-range order is observed in materials with a low-dimensional magnetic character, where strong magnetic interactions between the nearest ions are along the chains [32]. To understand more

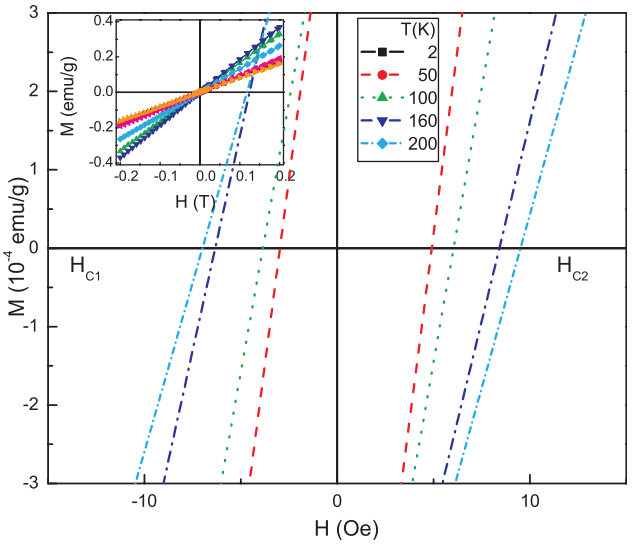

Figure 10 (online color at: www.pss-b.com) Isothermal magnetization measurements *M–H* from 2 to 200 K are shown in the main panel. The inset shows the magnetization at high field and different temperatures from 2 to 200 K. At low fields (main panel) the hysteretic effect is clearly observed. The asymmetric behavior in the coercive field might be related to a exchange bias effect due to an uncompensated or canted antiferromagnetism, but other types of interaction are not discarded such as that driven by Dzyaloshinsky–Moriya (DM)-type exchange.

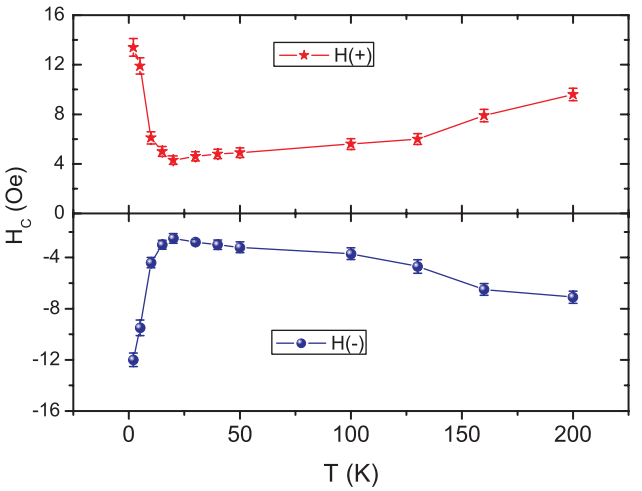

Figure 11 (online color at: www.pss-b.com) Coercive field versus temperature as determined by isothermal magnetic measurements for sample S4. Note the minimum at about 20 K.

about the magnetic characteristics of this oxalate, we studied the *M–H* isothermal measurements in the temperature range from 2 to 200 K; the resulting data is shown in Fig. 10 for the sample S4.

As can be noted in the inset of Fig. 10, the magnetization never reaches a saturation value; the *M–H* curve has almost a linear form, thus having the characteristic of AF order. However, a careful observation at low fields shows a small, but measurable, hysteretic behavior.

In order to clarify the existence of the hysteretic effect, studies of the coercive field H_C as a function of temperature were performed. Figure 11 shows H_C versus T for sample S4. Here we see the evidence of the asymmetric behavior related to the coercive field, thus implying an exchange bias effect $H_{C1} \neq H_{C2}$ due to two competing magnetic orderings: AF and WF. All studied samples have similar behavior. This exchange bias can be explained as the effect of inter- and intrachain interactions in this compound. The effect of interaction of metallic ions between chains is to cant the spins. This small but measurable exchange bias indicates that in place of having a pure antiferromagnetic order the magnetic order will be distorted by uncompensated antiferromagnetism due to the canted spins. Thus, two magnetic orders will be the result: a canted antiferromagnetism and a weak ferromagnetism. It is important to mention that great care was taken when measuring the exchange bias. Our SQUID magnetometer is provided with mu-metal shielding. At the moment of performing the magnetization measurements a flux gate magnetometer was used to demagnetize the superconducting coil. This procedure reduces the magnetic field to a very small value of about 0.001 G or less and the mu-metal shielding eliminates external magnetic influences, such as the Earth's magnetic field.

In Fig. 11, we observe that at 2 K the coercive field is about +13 Oe and decreases rapidly to a minimum value of 3 Oe, at temperatures close to 20 K. Above 20 K the coercive field increases in a smooth form reaching a value of 8 Oe at room temperature. This small but measurable coercive field clearly indicates a system with canted spins and thus a competition between possible DM interaction antiferromagnetism and weak ferromagnetism.

Evidently, the situation at low temperatures is more complicated. Analysis of the susceptibility data for cobalt(II) complexes may show deviation from simple Curie–Weiss behavior [31] by different mechanisms: single-ion, orbital moments, spin–orbit coupling, distortions from regular stereochemistry and crystal field, and also DM interactions. All these processes clearly may affect the magnetic properties.

The ground state of the free Co(II) ion is ^4F, but the orbital degeneracy is removed in an octahedral crystal field giving a $^4T_{1g}$ ground state. The combined effect of the spin–orbit coupling and the axial or rhombic distortions of the crystal field most often gives rise to six Kramers doublets; two are much lower in energy. When the temperature is low enough, only the ground Kramers doublet is thermally populated and the Co(II) ion can be formally treated with an effective spin $S = 1/2$ and a very anisotropic $\boldsymbol{g}$ tensor [28]. In the case of β-$CoC_2O_4 \cdot 2H_2O$ this temperature is low enough and is close to 7.5 K.

Reports on magnetic studies of some chain and layered six-coordinated cobalt(II) compounds [6, 31] show that, at low temperature, these magnetic systems behave as a collection of Ising chain with $S = 1/2$ effective spins coupled ferromagnetically and/or with antiferromagnetic

interactions [31]. It is necessary to note that the Ising model is restricted to the temperature range where only the ground Kramers doublets are thermally populated; thus, $T < 40$ K. However, at high temperatures a crossover to the Heisenberg-type behavior is expected.

4 Conclusions Microcrystals of cobalt(II) oxalate were prepared by soft solution chemistry. Powder XRD patterns show an orthorhombic phase. Chemical analysis, DTA, and TG studies revealed that the microcrystals have high purity. χ–T measurements reveal the existence of an AF ordering, by interaction of coupled chains via inter- and intrachain interactions and/or DM-type exchange. Those effects of interchain interaction affect the AF coupling, distorting it and canting the spins producing a weak ferromagnetic ordering. These WF and canted AF are evident by hysteresis measurements in M–H studies.

Acknowledgements Partial support for this work is gratefully acknowledged to CONACyT, Project No. 44296/A-1 and Scholarship CONACyT, Register No. 188436 for E. Romero; and VIEP-BUAP, Project No. MEAM-EXC10-G. We also thank F. Morales for providing the heat capacity measurements.

References

[1] S. Decurtins and M. Verdaguer, Philos. Trans. R. Soc. Lond. A **357**, 3025 (1999).
[2] J. S. Miller and A. J. Epstein, MRS Bull. **25**, 21 (2000).
[3] V. I. Ovcharenko and R. Z. Sagdeev, Russ. Chem. Rev. **68**, 345 (1999).
[4] A. R. West, Solid State Chemistry and its Applications (John Wiley, New York, 1984), p. 553.
[5] S. J. Blundell and F. L. Pratt, J. Phys.: Condens. Matter **16**, R771 (2004).
[6] S. Simizu, J. Y. Chen, S. A. Friedberg, J. Martinez, and G. Shirane, J. Appl. Phys. **61**, 3420 (1987).
[7] N. S. Ovanesyan, G. V. Shilov, A. A. Pyalling, C. Train, P. Gredin, M. Gruselle, L. F. Kiss, and L. Bottyán, J. Magn. Magn. Mater. **272**, 1089 (2004).
[8] K. Awaga, E. Coronado, and M. Drillon, MRS Bull. **25**, 52 (2000).
[9] M. B. Hursthouse, M. E. Light, and D. J. Price, Angew. Chem. Int. Ed. **43**, 472 (2004).
[10] T. D. Keene, H. R. Ogilvie, M. B. Hursthouse, and D. J. Price, Eur. J. Inorg. Chem. **2004**(5), 1007–1013 (2004).
[11] D. J. Price, A. K. Powell, and P. T. Wood, J. Chem. Soc. Dalton Trans. **2000**(20), 3566–3569 (2000).
[12] M. Kurmoo, Chem. Soc. Rev. **38**, 1353 (2009).
[13] J. Bacsa, D. Eve, and K. R. Dunbar, Acta Crystallogr. C **61**, m58 (2005).
[14] R. Deyrieux, C. Berro, and A. Péneloux, Bull. Soc. Chim. Fr. **1**, 25 (1973).
[15] P. J. Dubernat and H. Pezerat, J. Appl. Crystallogr. **7**, 378 (1974).
[16] M. Molinier, D. J. Price, P. T. Wood, and A. K. Powell, J. Chem. Soc. Dalton Trans. **1997**(21), 4061–4068 (1997).
[17] R. Deyrieux and A. Péneloux, Bull. Soc. Chim. Fr. 2675–2681 (1969).
[18] C. Drouet, A. Pierre, and A. Rousset, Solid State Ionics **123**, 25 (1999).
[19] I. Sledzinska, A. Murasik, and P. Fisher, J. Phys. C, Solid State Phys. **21**, 5273 (1988).
[20] G. A. Bain and J. F. Berry, J. Chem. Educ. **85**, 532 (2008).
[21] O. Pujol, P. Bowen, P. A. Stadelmann, and H. Hofmann, J. Phys. Chem. B **108**, 13128 (2004).
[22] N. Jongen, P. Bowen, J. Lemaitre, J. C. Valmalette, and H. Hofmann, J. Colloid Interface Sci. **226**, 189 (2000).
[23] S. Vaidya, P. Rastogi, S. Agarwal, S. K. Gupta, T. Ahmad, A. M. Antonelli, K. V. Ramanujachary, S. E. Lofland, and K. Ganguli, J. Phys. Chem. C **112**, 12610 (2008).
[24] T. Sugimoto and E. Matijevic, J. Colloid Interface Sci. **74**, 227 (1980).
[25] G. H. Ayres, Anlisis Qumico Cuantitativo (Ed. Harla, México, 1970), p. 59.
[26] L. B. McCusker, R. B. Von Dreele, D. E. Cox, D. Louër, and P. Scardi, J. Appl. Crystallogr. **32**, 36 (1999).
[27] W.-W. Wang and Y.-J. Zhu, Mater. Res. Bull. **40**, 1929, (2005).
[28] J. A. Lukin, S. Simizu, N. S. VanderVen, and S. A. Friedberg, J. Magn. Magn. Mater. **140**, 1669 (1995).
[29] J. C. Bonner and M. E. Fisher, Phys. Rev. **135**, A640 (1964).
[30] J. Glerup, P. A. Goodson, D. J. Hodgson, and K. Michelsen, Inorg. Chem. **34**, 6255 (1995).
[31] U. García-Couceiro, O. Castillo, A. Luque, G. Beobide, and P. Román, Inorg. Chim. Acta **357**, 339 (2004).
[32] D. J. Price, A. K. Powell, and P. T. Wood, J. Chem. Soc. Dalton Trans. **2003**(12), 2478–2482 (2003).